Available online at www.sciencedirect.com
SCIENCE DIRECT®
International Journal of Heat and Fluid Flow 24 (2003) 551–561
International Journal of HEAT AND FLUID FLOW
www.elsevier.com/locate/ijhff

Towards the prediction of noise from jet engines

M.L. Shur [a,*], P.R. Spalart [b], M.Kh. Strelets [a], A.K. Travin [a]

[a] Federal Scientific Center "Applied Chemistry", 14 Dobrolyubov Avenue, St. Petersburg 197198, Russia
[b] Boeing Commercial Airplanes, Seattle, WA 98124, USA

Received 23 November 2002; accepted 5 March 2003

Abstract

We are in the initial stages of development of a "non-empirical" numerical tool for jet-noise prediction in the airline industry, ultimately to treat complex nacelles and nozzles. The non-empirical demand leads to compressible large-eddy simulations, followed by post-processing to produce the far-field sound. Here we treat a simple cold jet with an axisymmetric geometry. The simulations leave out the subgrid-scale model (which causes too much dissipation on the present grid as is often the case in transitional flows), use slightly upwind-biased high-order differencing, and are preliminary in that a grid-refinement has not yet been performed. We do not use any unsteady forcing. The initial instability remains grid-sensitive, but the region with developed turbulence gives accurate statistics. The sound seen in the simulations is also realistic. The far-field sound calculations use the Ffowcs Williams–Hawkings (FWH) equation with a control surface that encloses the turbulence as much as possible, and the outside quadrupoles omitted. We focus on the influence of the surface location and the problem of closing the FWH surface at the outflow of the simulation. Though many physical and numerical issues are only partly resolved, the agreement with experiment is quite good for the sound's level, directivity, and spectral content.

Keywords: Turbulent jets; Large eddy simulation; Far-field noise; Ffowcs Williams–Hawkings equation

1. Introduction

Our motivation to reduce airliner noise is higher than ever. However the room for further by-pass-ratio increases, bringing about both noise improvement and performance benefits, is now very narrow, and we have to trade cost or performance for silence. This might involve setting the fan diameter or nozzle length beyond the cost optimum, or building non-circular nozzles, with "chevrons" on their trailing edge or any other devices that reduce jet noise at an acceptable performance/cost penalty. The evaluation of such devices at a design stage, or a noise prediction sufficient for certification, are near impossible without a very capable computational tool for far-field noise prediction. The available methods rest on scaling laws such as Lighthill's based on the engine's dominant parameters, or on constructs based on steady CFD solutions with two-equation turbulence models. These involve numerous empirical steps, particularly in synthesizing noise sources from just two turbulent parameters and a mean deformation tensor. There is no basis to expect that they remain accurate with streamwise vortices injected by chevrons, other new flow features due to design innovations, nor even wide temperature variations. Screech and shock-cell noise further challenge these methods.

We consider that only methods that calculate the sound from first principles starting via large-eddy simulations (LES) coupled with integral (Kirchhoff or Ffowcs Williams–Hawkings) methods for the far-field noise evaluation have real promise. Though such studies are active in the academic circles with large grids (at least several million nodes) and high-order numerics for simple jets (see, for example, Freund et al., 1998; Bogey et al., 2000; Constantinescu and Lele, 2001; Freund, 2001), they will not lead directly to a tool of industrial "strength" in a few years. This must include the ability to treat high-Reynolds number two-stream jets, in flight, with the nacelle and chevrons or similar features. This jet noise is in addition to combustion noise, fan noise, and other sources, which require different tools. Screech

* Corresponding author. Tel./fax: +7-812-238-9827.
E-mail address: michael_shur@mail.ru (M.L. Shur).

0142-727X/03/$ - see front matter © 2003 Published by Elsevier Science Inc.
doi:10.1016/S0142-727X(03)00049-3

Nomenclature

A_{r05}	rate of jet half-radius growth
B_u	rate of jet centerline-velocity decay
c	sound speed
D	nozzle diameter
f	frequency
M	Mach number, U_{jet}/c_0
n	vector of outward normal
n_j	projections of vector **n** on coordinate axes
r	radial coordinate, $(y^2+z^2)^{1/2}$
p	pressure
St	Strouhal number, fU_{jet}/D
t	time
T	temperature; length of time sample
T_{ij}	components of Lighthill's tensor
u, v, w, u_j	velocity components
U_{jet}	jet velocity
u_n	normal velocity component
V	volume outside FWH control surface
x, y, z, x_j	Cartesian coordinates
x	observer radius-vector
y	field point radius-vector
γ	specific heat ratio
δ, δ^*	incoming boundary layer thickness and momentum thickness
Δt	time-step
Δx, Δr, $\Delta\varphi$	grid spacing
$\Delta\tau$	time-step of FWH data saving
θ	angle between jet axis and observer radius-vector
λ	wave-length
ρ	density
Σ	control FWH surface
τ_r	retarded time
φ	polar angle
ω	angular frequency, $2\pi f$
Subscript	
0	ambient (still air) parameters
Superscript	
$'$	acoustic and turbulent perturbations

and shock-cell noise will be amenable to the present method, although shocks may defeat the high-order differencing that is customary in LES. Both the frequency spectrum and the directivity are essential with a desired accuracy of about 2–3 dB. The frequency range of interest extends, roughly, from 10 Hz up to 4 kHz, which puts much pressure on the range of scales to be resolved in the CFD of the flow and on the algorithm used for extracting far-field sound.

In this paper we outline the initial development of the tool. In Section 2 we succinctly present the approaches used for flow and far-field sound computation. Then, in Section 3, we outline the major results obtained to date for simple round jets. In Section 4, we discuss issues, which arose in the course of the study, and prospects for further work.

2. Numerical approaches for jet-flow and far-field noise computation

2.1. Jet-flow simulation

The NTS code (Strelets, 2001) is capable of treating quite general geometries, with multi-block structured grids, and a wide range of Mach numbers. The Navier–Stokes flow solver is based on an optional (upwind biased or centered) high-order finite-volume approximation in space, and on a second-order three-layer implicit procedure in time. The upwind part of the scheme uses the flux-difference splitting algorithm of Roe (1981). More specifically, for the inviscid fluxes, F, we use the fifth-order upwind and the fourth-order centered schemes with a geometry-dependent weight function, σ_{upw}:

$$F_{hybrid} = \sigma_{upw}F_{upw} + (1-\sigma_{upw})F_{central}.$$

For the viscous fluxes, the centered second-order approximation is used.

The weight function used in the computations is shown in Fig. 1. It provides a gradual switch towards the centered scheme starting at the plane of the nozzle exit ($x=0$) and ending at $x=D$ (D is the nozzle diameter) where the weight of the upwind part reaches its minimum value $(\sigma_{upw})_{min}=0.25$. As a result, the scheme is operating as an effectively centered one in the most active turbulent and mid-acoustic regions where the highest resolution is needed. If $(\sigma_{upw})_{min}$ is lowered further, the solution in the turbulent-acoustic interface becomes highly non-monotonous, and therefore unusable. This occurs with the rather high Reynolds number we are using, as discussed shortly.

With the use of the above numerics we have been running a "coarse-grid direct numerical simulation" (DNS) by which we mean a numerical solution of the three-dimensional unsteady Navier–Stokes equations on grids that are too coarse to claim a "true" DNS but still capable of providing a sufficient resolution of the major

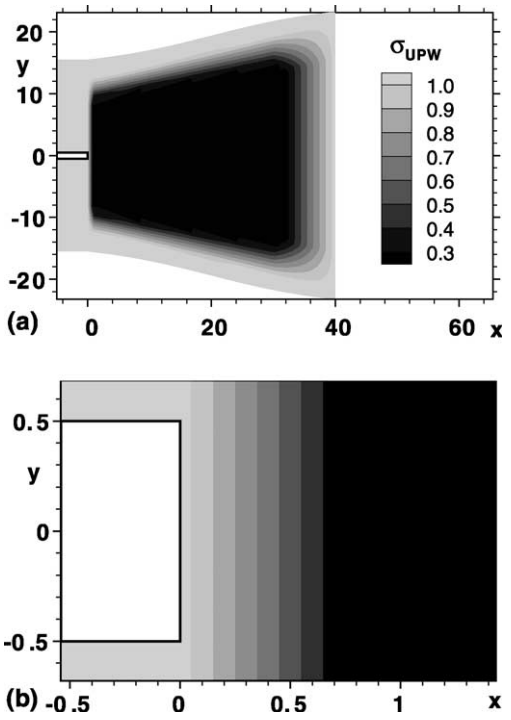

Fig. 1. *xy*-cut of the weight function contours (a) and its enlarged fragment (b).

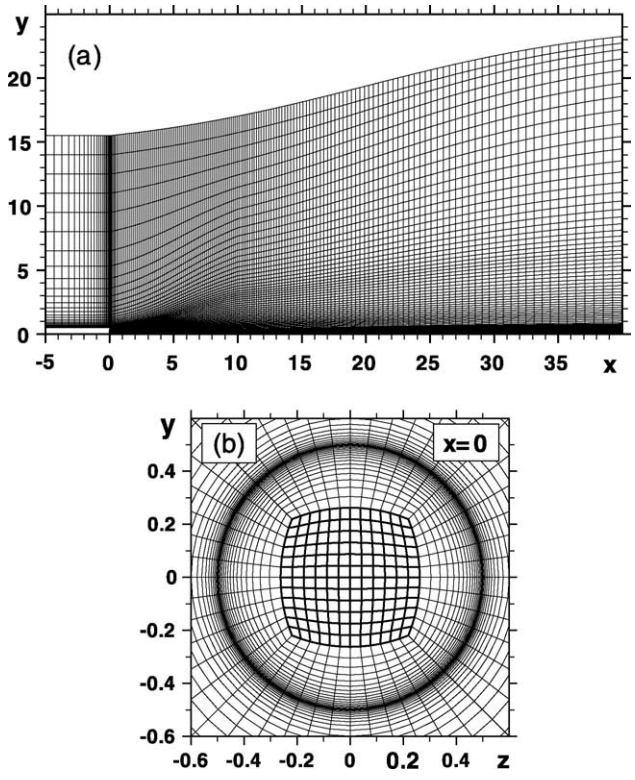

Fig. 2. Computational grid in *xy*-plane (a) and its enlarged fragment in *yz*-plane (b); bold lines: inner block, thin lines: outer block.

flow-structures responsible for the noise generation. The approach is similar to that called monotonically integrated LES (MILES), which is known to be rather successful as applied to the free shear flows (Oran and Boris, 2001), but is not exactly MILES, since the numerical method we use is not strictly monotonic. Our motivation for this is to obtain velocity fields rich enough to exercise the sound calculation with a manageable grid and the possibility of running many cases. We reserve true LES, detached-eddy simulation (Spalart et al., 1997), or may be some other hybrid approach for more complex real life geometries.

The grid we used (see Fig. 2) has a two-block topology that seems optimal for axisymmetric jets. The inner block (which has $151 \times 13 \times 13$ nodes) is helpful to avoid a singularity at the axis of the cylindrical coordinates. The outer, O-type, block has $171 \times 52 \times 49$ nodes in the streamwise, radial, and azimuthal directions respectively which resulted in a total number of nodes ≈500,000. The simulations were performed at the Reynolds number 10^4, while the limit for well-resolved DNS with this grid is closer to 2×10^3. Consequently we make no claim to grid-independent solutions although, as shown below, the present grid and numerics predict the turbulence statistics in the developed jet region with a very acceptable accuracy (upstream of that region, we do not have reference data with sufficient knowledge of the inflow conditions).

2.2. Boundary conditions and near-boundary treatment

The design of non-reflective inflow/outflow boundary conditions and other tools aimed at suppressing the errors caused by reflections from the boundaries, e.g., sponge-like layers of different kinds (Freund, 1997; Zhao et al., 2000; Ashcroft and Zhang, 2001), is a challenging CFD issue that is especially important when the final goal of a simulation is sound prediction. Another challenge is the formulation of physically correct inlet conditions that provide a realistic flow behavior in the jet entry region. In the present work the following set of boundary conditions and near-boundary treatment has been implemented.

At the left boundary ($x = -5$, $|r| > 0.5D$ and $x = 0$, $|r| < 0.5D$) we impose profiles of the normal velocity and temperature, and set the tangential velocity to zero. To set the pressure we use the one-dimensional non-reflecting boundary condition proposed by Engquist and Majda (1977) $\partial p/\partial t + (u - c)\partial p/\partial x = 0$ (c is the local speed of sound).

At the "funnel-shaped" lateral boundary of the domain we use extrapolation for the radial velocity, u_r. The velocity vector may point into the domain, or outwards, making it locally an "inlet" or an "outlet" region. At the outlet points of the funnel, we extrapolate the other two velocity components and the quantity p/ρ^{γ} and compute

the speed of sound as $c = 0.5(c_{\text{extr}} + c_0)$, where c_{extr} is a value obtained by linear extrapolation from the interior grid nodes and c_0 is the speed of sound in the ambient air.

At the inlet points of the funnel we impose the streamwise velocity, u_x, equal to the desired co-flow velocity (zero in the present paper) and set the azimuthal component, u_φ, to zero. Other than that, we assume that the ambient parameters (p_0, T_0, ρ_0) are known and use "isentropic" relations $p/\rho^\gamma = p_0/\rho_0^\gamma$ and $T/T_0 = [1 + 0.5(\gamma - 1)(u_r/c)^2]^{-1}$.

At the right boundary we impose the first order zero x-derivative condition for all the variables, including pressure. Though such conditions are mathematically sub-optimal, they still work thanks to holding the pressure at the funnel. Also, these conditions are the only ones we tried that tolerate the events of negative streamwise velocity associated with jet turbulence in a zero co-flow.

In order to avoid or, at least, to weaken the reflections which are inevitable with the above (and probably with any other) boundary conditions, we place an "absorbing" stationary layer along all the boundaries, except for the nozzle exit. The idea originates with Freund (1997), and the simple implementation we use in the present work was suggested by Ashcroft and Zhang (2001). It consists in a smooth matching of a real and a "target" flowfield within the layer with the use of the relation

$$F(l) = (1 - s) \cdot F(l) + s \cdot F_{\text{target}}(l).$$

Here F is the "real" flow quantity (from the solution on the current time step) at the considered point, F_{target} is the corresponding target quantity at the same point, $s = (l/L)^\beta$, L is the width of the layer, and l is the distance from the internal boundary of the layer to the considered point ($0 < l < L$). The values of the control parameters adjusted in the course of preliminary simulations are as follows: $\beta = 3$, $L = 10D$ at the outflow boundary, $5D$ at the funnel, and $3D$ at the left boundary ($x = -5D$). Finally, the target solution we used was just an arbitrary instantaneous flowfield from the simulation at $t > 500D/U_{\text{jet}}$ (a test using instead the time- and φ-averaged solution as a target flow-field showed no visual difference). In addition to the use of the absorbing layer, in order to speed up damping of the disturbances in the near boundary region, within the absorbing layer, the order of the upwind part of the scheme is changed from fifth to third.

It should be emphasized that in contrast with most studies in the literature that use unsteady forcing at the nozzle exit, often involving many Fourier modes in time and space as well as random shifts, we preferred to perform simulations with steady inlet boundary conditions. This avoids both the introduction of arbitrary parameters and the necessity to filter out the "false" noise created by the artificial forcing. Thus, we impose a steady uniform velocity profile with the thin boundary layer. Nonetheless, the flow comes out realistic, i.e., we do observe all the features typical of the initial region of jets at high Reynolds numbers (the shear layer roll-up, vortex pairing, flow three-dimensionalisation, and fast transition to turbulence). On the other hand, we do realize that this behavior is numerics/grid-dependent at the present levels of resolution, Reynolds number, and shear-layer thickness. As an illustration, in Fig. 3 we show vorticity snapshots from simulations with the nominal and a delayed switch from upwind-biased to centered scheme (starting at $x = 2D$ instead of $x = 0$). We know also that full-size flows should have "LES content" (i.e., resolved eddies) in the incoming boundary layers which may be a key to a more reproducible transition process (since the turbulence will obey normal boundary-layer physics), but the compromises between resolution and realism will be difficult. Even an LES (say, with the Smagorinsky or SA subgrid model; Shur et al., 1999) of the jet without a nozzle is much more demanding in terms of the computer resources than the coarse-grid DNS we are employing in this study. This is demonstrated in Fig. 4, where we present a comparison of vorticity snapshots obtained from coarse-grid DNS and from LES with the SA subgrid model. The figure clearly indicates that in LES, transition to turbulence is delayed by many diameters, even though the grid is capable of resolving the shear layer roll-up. This is due to the inability of subgrid models to distinguish the mixing-layer conditions from the inertial-range conditions they were adjusted for. The only immediate solu-

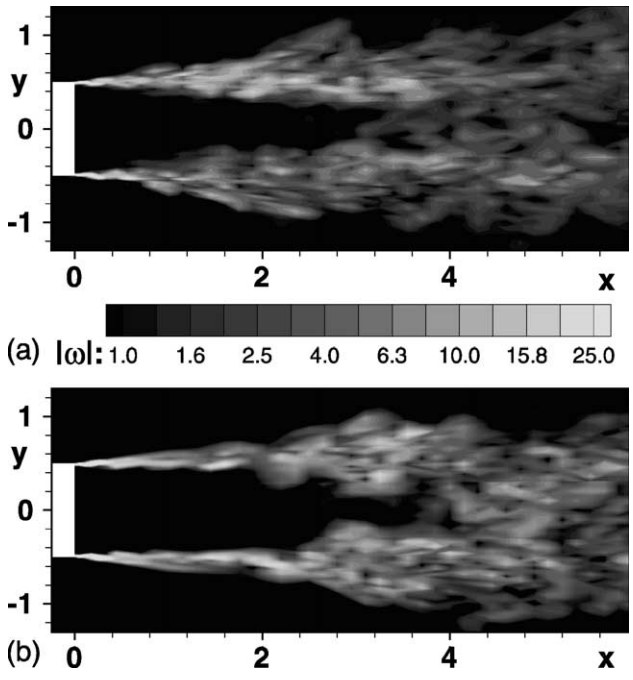

Fig. 3. Vorticity snapshots with the nominal (a) and delayed (b) start of switching to the centered scheme.

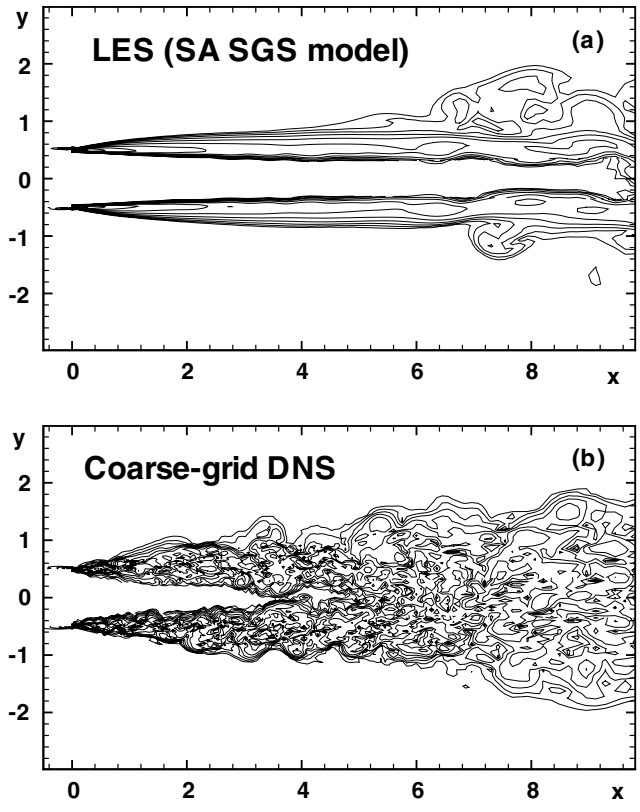

Fig. 4. Vorticity snapshots from LES with SA subgrid model and from coarse-grid DNS.

tions would be to strongly refine the grid, or to arbitrarily weaken the SGS model.

2.3. Acoustic post-processor

For the evaluation of the far-field sound we use the Ffowcs Williams–Hawkings (FWH) equation, which seems to be the best compromise between numerical efficiency and accuracy. For the present case of a jet with no co-flow, the FWH theory (Ffowcs Williams and Hawkings, 1969), which generalizes Lighthill's (1952) acoustic analogy, gives the following relation for the far-field acoustic pressure, $p' = p(\mathbf{x}, t) - p_0$ (Dowling, 1992):

$$4\pi|\mathbf{x}|p'(\mathbf{x},t) = \frac{x_j x_l}{|\mathbf{x}|^2 c_0^2}\frac{\partial^2}{\partial t^2}\left[\int_V \{T_{jl}\}\,\mathrm{d}V\right] + \frac{x_j}{|\mathbf{x}|c_0}\frac{\partial}{\partial t}\left[\int_\Sigma \{p' n_j + \rho u_j u_n\}\,\mathrm{d}\Sigma\right] + \frac{\partial}{\partial t}\left[\int_\Sigma \{\rho u_n\}\,\mathrm{d}\Sigma\right]. \quad (1)$$

Here vector $\mathbf{x}$ defines an observer position; Σ is the FWH surface; V is the volume outside Σ; the quantities in square brackets are computed at the "retarded" time, i.e., at the moment when the sound was generated $\tau_r = t - |\mathbf{x} - \mathbf{y}|/c_0$ where $\mathbf{y}$ is the coordinate of the current field point ($\tau_r \approx t + x_j y_j/(|\mathbf{x}|c_0) + \text{const}$ in the "far-field", i.e., at large $|\mathbf{x}|/|\mathbf{y}|$); n_j are the projections of the vector of outer normal to Σ, $\mathbf{n}$, on the coordinate axes; $T_{jl} = \rho u_j u_l + p_{jl} - c_0^2\rho'\delta_{jl}$ is the Lighthill tensor; $\rho' = \rho - \rho_0$ is the acoustic density; $p_{jl} = p\delta_{jl} - \tau_{jl}$ is the total stress tensor; τ_{jl} is the viscous stress tensor; u_j are the velocity components, and u_n is the velocity component normal to the surface. In high-Reynolds-number flows the viscous term in the Lighthill's tensor is often omitted which results in the relation $T_{jl} = \rho u_j u_l + (p' - c_0^2\rho')\delta_{jl}$. However, we note that in LES, SGS stresses vanish only as the grid spacing vanishes; this is an additional incentive to place Σ in an area that removes the need to involve this tensor.

If all the noise sources are located inside the surface Σ, then the first, quadrupole, term in the right-hand side of Eq. (1) can be omitted which results in a crucial simplification of the solution procedure. The database is three- rather than four-dimensional. The principal difficulty in jet cases, as opposed to the cases of "isolated turbulence" considered by Lighthill, is dealing with the slow decay of the turbulence downstream, which means that T_{jl} does not accurately fall to zero within a manageable distance. This will be even worse with a co-flow, unless the convection of weak turbulence by a non-zero co-flow can be used to advantage to approximate the contribution of the missing region.

In the course of the flow simulation, the surface integrands in the right-hand side of (1) are saved with a time interval $\Delta\tau$, and a dedicated acoustic post-processor performs a numerical Fourier transform (FT) of Eq. (1). As a result, we obtain the FT of the acoustic pressure $\hat{p}(\mathbf{x}, f_n)$ for the discrete set of frequencies $f_n = n/(N\Delta\tau)$, $n = 0, 1, \ldots, N/2$ (N is the number of fields saved in the time-sample) and for different observer directions (θ, φ). After averaging of that quantity over the polar angle φ, we get the amplitude of the far-field acoustic pressure as a function of the non-dimensional frequency $St = fD/U_{\text{jet}}$ and observer position, θ (θ is the angle between the jet axis and the radius-vector of the observer $\mathbf{x}$).

It should be emphasized that, when we first implemented the technique briefly outlined above, we were faced with very inaccurate sound predictions when the FWH surface was closed at the downstream end (thus including a "closing disk"), which is, strictly speaking, necessary to be consistent with the fundamentals of the approach. Predictions with the surface left open were much closer to experiments. A study of this issue showed that the errors are associated with the computation of the time derivatives in (1) in Fourier space with the use of relation $\mathrm{FT}(\partial\psi/\partial t) = -\mathrm{i}\omega\mathrm{FT}(\psi)$. This is explained by non-periodicity of the signal $\psi(t)$ which leads to a discontinuity if, as it is assumed by the FT, the signal values at the ends of a time sample are simply "connected". At the outlet disk, for any reasonable length of the computational domain, the amplitude of the

discontinuity turns out rather large. This results in a large spike in the time-derivatives, which invades the entire spectrum. Probably, a properly tuned "windowing" procedure similar to that used by Freund (2001) can eliminate this deficiency of the Fourier-space computation of the time derivatives. However in this work we preferred another approach, namely, to compute the derivatives in the time domain instead. The windowing procedure demands an adjustment of the window parameters, longer time samples, and, last but not least, does not permit to get a good preliminary estimate of the sound based on relatively short time samples (~50 convective units) as is quite possible when the derivatives are computed in the time domain.

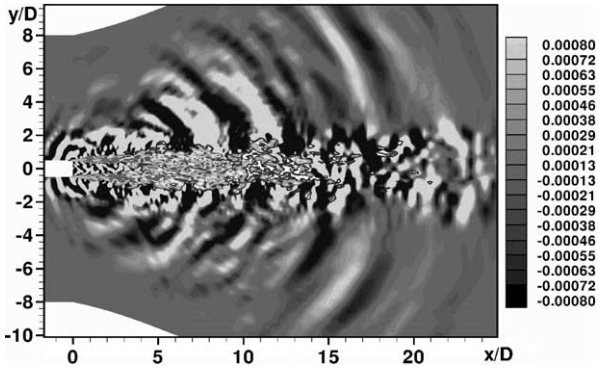

Fig. 5. Snapshot of pressure time-derivative (normalized with c_0, ρ_0, D), shaded, and vorticity, lines and shades, from simulation at Mach 0.9.

3. Results and discussion

With the techniques outlined above we performed a simulation of a round jet at a Reynolds number of 10^4 based on jet diameter and velocity, Mach number $M = U_{\text{jet}}/c_0 = 0.9$, and boundary-layer momentum thickness $\delta^* \approx 0.004D$ (boundary layer thickness $\delta \approx 0.03D$). The time integration is performed with the step $\Delta t = 0.04D/U_{\text{jet}}$ and a complete simulation takes on the order of $t = 1000D/U_{\text{jet}}$. This case is close to real aircraft engines, in terms of Mach number, and has been studied both experimentally and numerically in a number of projects (e.g., Lush, 1971; Tanna, 1977; Stromberg et al., 1980; Freund, 2001; Constantinescu and Lele, 2001; Zhao et al., 2001).

The first issue we addressed was whether incompressible simulations are usable for the evaluation of a subsonic jet's far-field sound through Lighthill's acoustic analogy. It turned out that even at low Mach numbers the pressure disturbances in the acoustic range in the compressible and incompressible simulations differ drastically. In particular, the pre-turbulent flow unsteadiness (shear layer roll-up and vortex pairing) and turbulence create waves centered on the mixing layer and at the end of the jet potential core, respectively (see Fig. 5). The latter waves, especially, radiate more strongly downstream. Those features are absent from the incompressible simulation and appear essential for a correct rendition of the far-field sound and, particularly, its directivity. We do not consider the question completely closed, in the sense that we did not try applying the full quadrupole treatment to an incompressible field (with an artificial speed of sound), but we note that most jets of interest on airliners have Mach numbers near 1, so that a Mach-number expansion should not be accurate. Airframe noise at low Mach numbers may be another matter.

We now consider the salient results of the simulation.

First, in Fig. 6, we present turbulence statistics; time averaging starts after running the flow for about 800 convective time units and covers 400 time units. The figure gives strong evidence that the grid and numerics used in the simulation are good enough for the developed turbulence (i.e., after the 3D breakdown and full flow chaotization). The agreement between the predicted and experimental mean-flow characteristics and Reynolds stresses in this region is very good. For instance, according to the simulation, the rate of centerline-velocity decay, B_u, and the rate of half-radius growth, A_{r05}, come out as 6.05 and 0.094 (dotted lines in Fig. 6a), while their experimental values vary in the ranges 5.4–6.1 and 0.086–0.096 respectively (Zaman, 1998). Therefore, as far as turbulence is concerned, we have confidence that the energy-containing motion is captured, and leave for later the question of whether the resolved frequency range is wide enough for the noise.

Before starting the analysis of the far-field sound predictions, some preliminary comments should be made on the specific FWH surfaces we have chosen. In order to evaluate the effect of their specific design and location, we have collected the FWH data for a rather wide set of different surfaces. All are funnel-shaped in order to fit the turbulent region, but they leave different clearances. Fig. 7 shows three representative surfaces of different width (***S*1**, ***S*2**, and ***S*3**) together with a snapshot of the magnitude of Lighthill's source term $|\partial^2 T_{jl}/\partial x_j \partial x_l|$ (we do not use this term in our integration, but view it as a diagnostic when assessing FWH surfaces). One can see that the sleeve of the ***S*3** surface is located very close to the boundary of the turbulent and mid-acoustic areas. The length of the surfaces, $x_{\text{end}} = 25D$, is the largest that avoids the sound deterioration caused by the special near-boundary approximations described above. Shorter surfaces of length $21D$ and $17D$ were considered as well. In addition, in order to evaluate the error caused by the use of open FWH surfaces (without closing disk), along with the described closed surfaces similar surfaces open at the outlet end were considered. The "tightest" un-closed surface, ***S*3*U***,

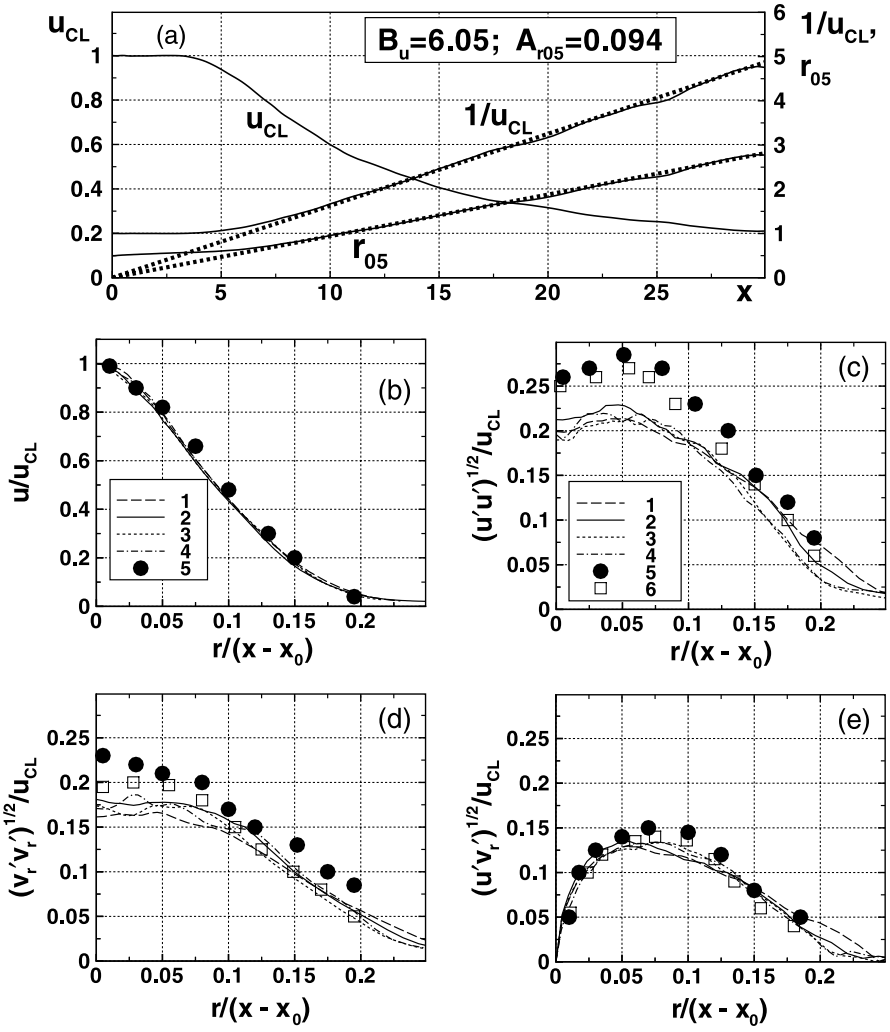

Fig. 6. Comparison of predicted mean flow parameters and Reynolds stresses with experiments: 1—$x/D = 10$, 2—$x/D = 15$, 3—$x/D = 20$, 4—$x/D = 25$; 5—Hussein et al. (1994); 6—Panchapakesan and Lumley (1993); velocity is averaged over all the grid points in yz-planes, stresses are averaged over y and z coordinate axes (four grid lines).

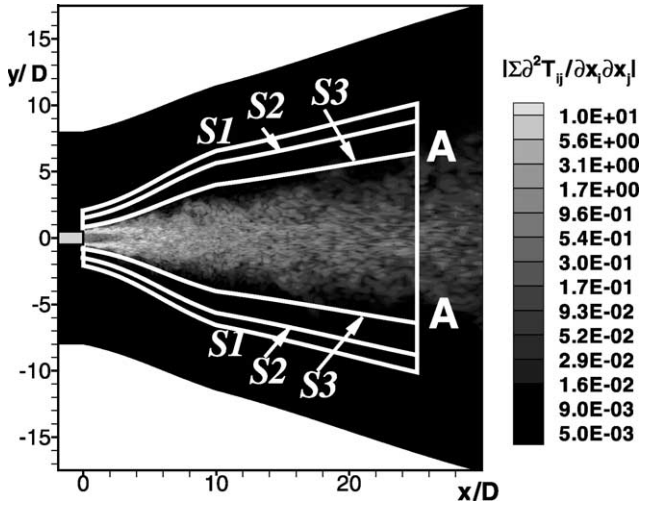

Fig. 7. FWH surfaces and snapshot of Lighhill's source term.

is obtained from the surface ***S3*** by a complete removal of the closing outlet disk. The other un-closed surfaces, ***S1U*** and ***S2U***, have at $x = x_{\text{end}}$ "hanging" vertical parts ending at the sleeve of ***S3*** (point "A" in Fig. 7) so that all three un-closed surfaces have the same "angle of vision" of the surface edge from the source of sound, θ_V, roughly equal to 20° (based on the simplified analysis of Freund et al. (1996) performed for open Kirchhoff surfaces, these surfaces should provide a correct noise prediction at observer angles larger than θ_V).

As far as the range of resolved frequencies is concerned, formally, it is bounded by the time step of saving the flow data for the noise computations, $\Delta\tau$, and by the length of the time sample, $T_{\text{sample}} : St_{\max} = 1/(2\Delta\tau)$. $St_{\min} = 1/T_{\text{sample}}$. Therefore, in our computations ($\Delta\tau = 5\Delta t = 0.2$; $T_{\text{sample}} = 200$), ideally, $St_{\min} = 0.005$ and $St_{\max} = 2.5$. However, in reality, the range is quite a bit narrower. First, the functions we are dealing with are far

from periodic in time. So we can anticipate resolving only the frequencies corresponding to periods being, say, 5–10 times less than the time sample which results in $St_{\min}$ being closer to 0.025–0.05. Second, due to the grid resolution restrictions, only those sound waves that are longer than, say, 4 grid cells can be resolved accurately enough, i.e., $St_{\max} < c_0/\lambda_{\min} < c_0/(4\Delta)$. However the grid cell size Δ is varying significantly along the FWH surface. For instance, at $x = 25$, $\Delta x \approx 0.4$, and so $St_{\max} \approx 0.7$. The radial grid step at $x = 25$, $\Delta r \approx 0.6$–0.8, and so $St_{\max} \approx 0.35$–0.5. Finally, the azimuthal grid step, $r\Delta\varphi$, at $r = 8$ is equal to ≈ 0.9, which results in $St_{\max} \approx 0.3$. These estimations show that the grid is far from sufficient for an accurate resolution of the high frequency sound. On the other hand, the major noise for the considered jet is generated in the frequency range $St \approx 0.1$–0.5. So even with that grid, we can hope for a quite acceptable accuracy for the integral sound intensity. Also, considering that the azimuthal waves are known to be weak and that the high-frequency sound is produced mostly in the entry region of the jet where the grid is relatively fine (even at the FWH surface, thanks to its shape), we still can expect to resolve frequencies up to $St_{\max} \approx 1.5$, provided that these contributions "enter" the far-field integrals in the better region of the grid. For these reasons, we present below the far-field sound spectra for the entire frequency range, while the overall sound intensity is computed only over the range $St = 0.05$–1.0. Note that widening the range to higher frequencies does not change the results noticeably since the signal drops steeply. Also, considering possible cancellations of contributions from different parts of an FWH surface, it is not clear whether resolving a high-frequency signal on only part of the surface leads to a smaller error in sound prediction than simply suppressing this frequency.

The major results of the far-field noise prediction are presented in Figs. 8–12. They turned out much better than we expected considering the grid coarseness, and

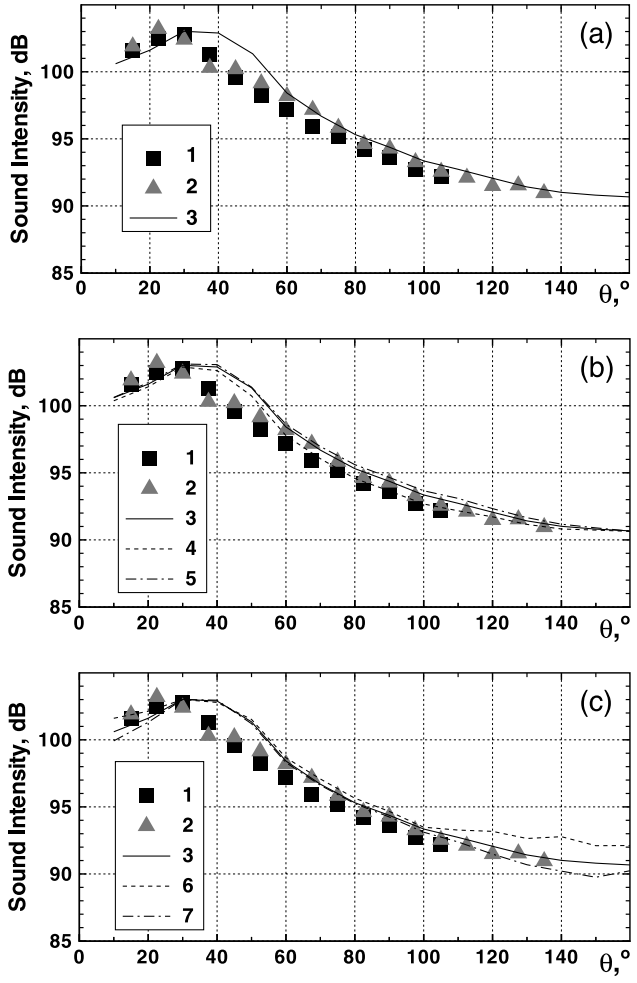

Fig. 8. Comparison with experiment (a) and effect of FWH surface width (b) and length (c) on the computed overall sound intensity at $|\mathbf{x}|/D = 120$: 1, 2—experimental data of Lush (1971) and Tanna (1977); 3, 4, 5—predictions with medium-long ($x_{\text{end}} = 21D$) surfaces ***S2*** (medium-wide), ***S3*** (narrow), and ***S1*** (wide); 6, 7—predictions with short ($x_{\text{end}} = 17D$) and long ($x_{\text{end}} = 25D$) surfaces ***S2***.

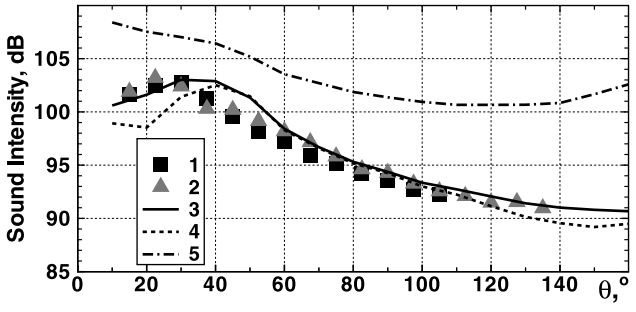

Fig. 9. Effect of the closing outlet disk and of the approach to the time-derivatives computation in the FWH post-processing on the overall intensity prediction: 1, 2, 3—as in Fig. 8; 4—prediction with un-closed surface ***S2U***; 5—prediction with closed surface ***S2*** and time-derivatives computed in the Fourier-space.

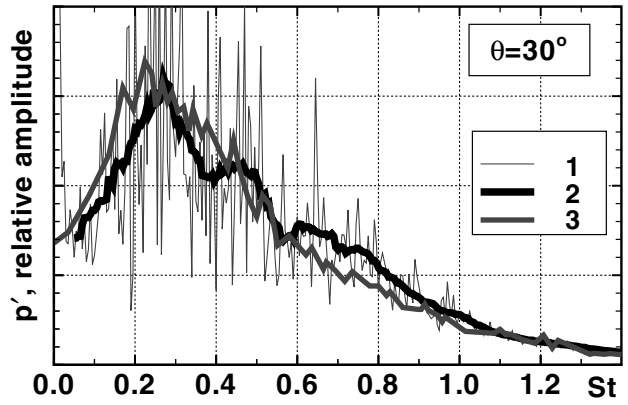

Fig. 10. Comparison of computed and measured acoustic pressure spectra; 1—"raw" spectrum, 2—"smoothed" (averaged over frequency interval $\Delta St = 0.1$) spectrum, 3—experiment of Stromberg et al. (1980).

appear better than those in the literature even with finer grids. In particular, as seen in Fig. 8a where we compare with the experiment the directivity of the overall sound intensity computed with the use of the medium-long ($x_{end} = 21D$) surface ***S2***, the discrepancy does not exceed 2 dB. Also, a very positive finding is that the FWH-surface sensitivity within the considered range is rather weak, unless the surface is too short, i.e., does not enclose the major sound sources (see Fig. 8b and c).

Fig. 9 confirms the importance of closing FWH surfaces at the downstream end for low observer angles, less than 35° (note that this angle is tangibly higher than

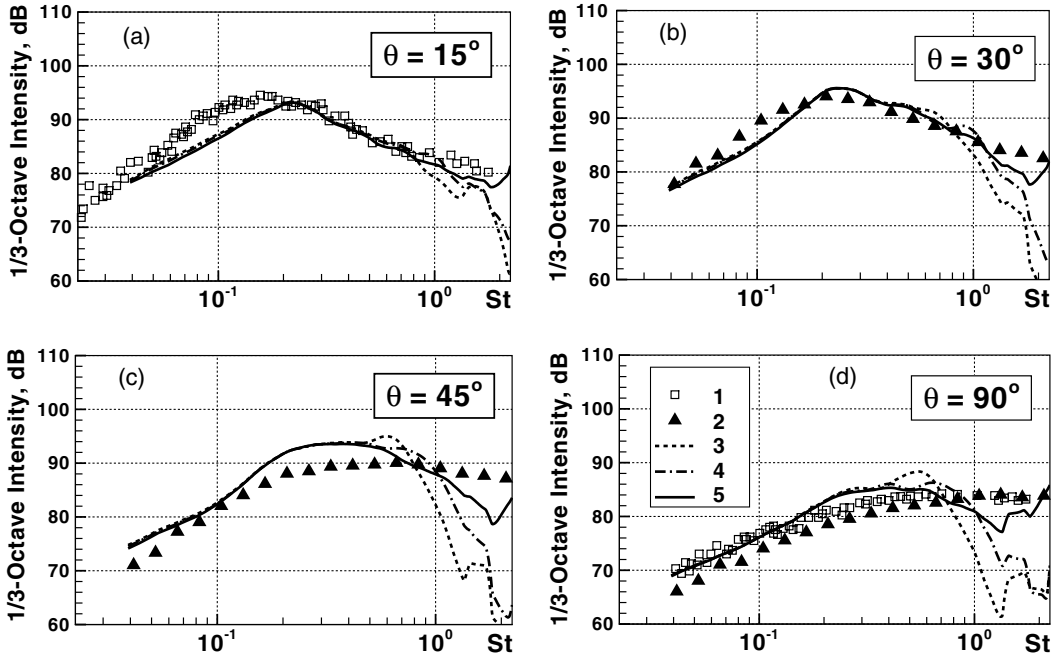

Fig. 11. Comparison with experiment and effect of the FWH surface width on the computed 1/3-octave sound intensities at $|\mathbf{x}|/D = 120$: 1, 2—experimental data of Lush (1971) and Tanna (1977); 3, 4, 5—predictions with medium-long ($x_{end} = 21D$) surfaces ***S1***, ***S2***, and ***S3***.

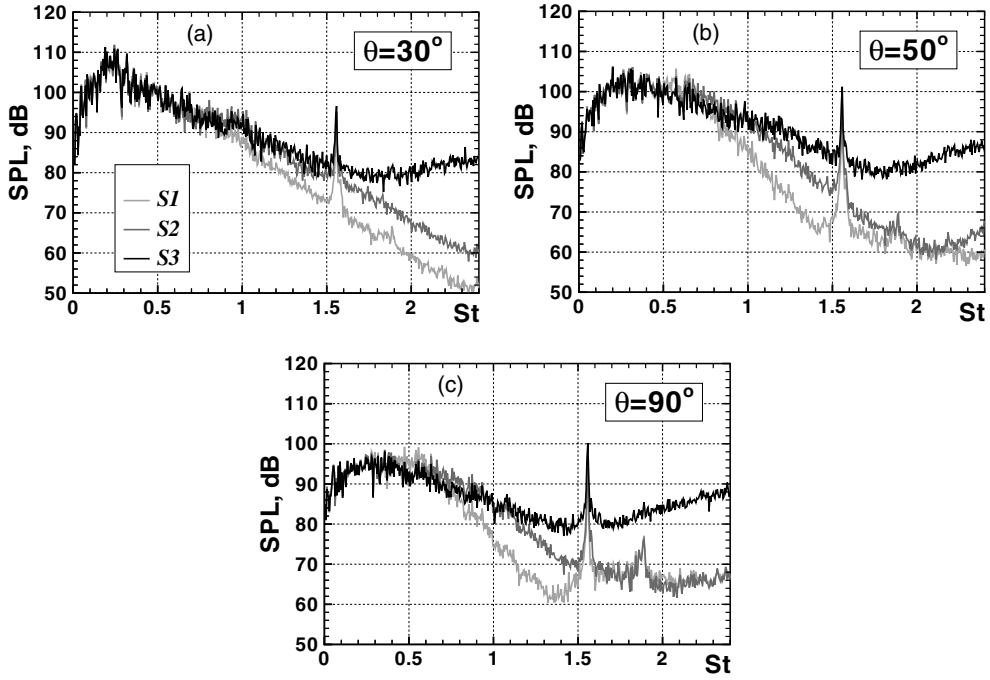

Fig. 12. Effect of the FWH surface width on SPL power spectra at $|\mathbf{x}|/D = 120$.

we estimated following Freund et al., 1996) and, also, the crucial role of the computation of the time derivatives at the closing disk in the time domain.

Figs. 10–12 show that the simulation captures not only the overall sound intensity, but also other salient features seen in experiments. Namely, it predicts broadband spectra and correct dominant frequencies. Also, as could be expected on the basis of the restrictions on the high-frequency wave resolution imposed by the grid discussed above, a significant sensitivity of the spectra to the FWH surface is observed only at high frequencies, $St > 0.7$. Exactly for this reason, this does not cause any noticeable surface-sensitivity of the overall far-field sound intensity, which, as mentioned above, is dominated by lower frequencies.

A peculiarity of the narrow-band sound pressure level (SPL) spectra presented in Fig. 12 is a tone at $St \approx 1.5$, corresponding to the shear layer roll-up. Such a tone is not observed in high-Reynolds-number jet experiments. Most probably, it is spurious and caused by the flow being too nearly axisymmetric and periodic upstream of transition. The tone may also be amplified by grid non-uniformities, which, as already discussed, can prevent the proper cancellation of signals from different parts of the FWH surfaces. If that is correct, the tone should get weaker or even go away with grid refinement.

4. Concluding remarks and outlook

A coarse-grid DNS of a round jet (total number of nodes around 500,000 for a Reynolds number of 10^4) has been performed at a Mach number of 0.9 primarily to evaluate the capabilities of this approach, coupled with the FWH technique, for the calculation of far-field sound. The ultimate goal of the study is a reliable, general, non-empirical CFD tool for prediction of the noise from jet engines. The product of the first stage of the study presented here is a numerical procedure that seems capable of providing the target accuracy of 2 dB for the overall far-field sound intensity generated by a simple subsonic jet. Important elements of the procedure are: a hybrid finite-difference method based on the fifth-order upwind/fourth-order centered scheme that functions as almost centered in the major part of the computational domain; a near-boundary treatment of the flow based on the use of an absorbing layer to prevent intense reflections from the boundaries; and a far-field noise post-processor based on the FWH approach without outside quadrupoles, with control surfaces closed by the disks at the outflow boundary, and with partial time-derivatives computed in the time domain rather than Fourier space.

On the other hand, many issues still should be resolved to reach our final goal. The simulations shown here are restricted to one value of the Mach number. We soon will explore Mach-number effects. The same is true for the effect of jet temperature, which is known to be significant for engines, and for the effect of a second stream, co-flowing ambient flow, and so on. The eventual industrial method will also account for sound reflection and refraction by the wing, for instance. The simulations have not included any representations of boundary-layer turbulence at the inflow. Though the differencing scheme and the present grid seem capable of providing the rapid transition to turbulence typical of high-Reynolds-number jets irrespective of the level of turbulence in the incoming boundary layers, this may be a key to a more reproducible transition process. The compromises between resolution and realism will be difficult. Our preliminary study of LES as applied to the present jet showed that the grids needed for that are unaffordable on our present computers. Still, activating the LES SGS model and therefore avoiding coarse-grid DNS is the key to approaching grid independence. This issue also will be addressed in future work.

Acknowledgement

The work is made possible by the Boeing Technology Research Center in Moscow.

References

Ashcroft, G., Zhang, X., 2001. A computational investigation of the noise radiated by flow-induced cavity oscillations. AIAA Paper, AIAA-2001-0512.

Bogey, C., Bailly, C., Juve, D., 2000. Computation of the sound radiated by a 3-D jet using large eddy simulation. AIAA Paper, AIAA-2000-2009.

Constantinescu, G.S., Lele, S.K., 2001. Large eddy simulation of a near-sonic turbulent jet and its radiated noise. AIAA Paper, AIAA-2001-0376.

Dowling, A.P., 1992. Effect of motion on acoustic sources. In: Modern Methods in Analytical Acoustics, Lecture Notes. Springer-Verlag, Berlin, pp. 406–426.

Engquist, B., Majda, A., 1977. Absorbing boundary conditions for the numerical simulations of waves. Mathematics of Computation 31, 629–651.

Ffowcs Williams, J.E., Hawkings, D.L., 1969. Sound generated by turbulence and surfaces in arbitrary motion. Phil. Trans. Royal Soc. A 264, 321–342.

Freund, J.B., 1997. Proposed inflow/outflow boundary conditions for direct computation of aerodynamic sound. AIAA J. 35, 740–742.

Freund, J.B., 2001. Noise sources in a low-Reynolds-number turbulent jet at Mach 0.9. J. Fluid Mech. 438, 277–305.

Freund, J.B., Lele, S.K., Moin, P., 1996. Calculation of the radiated sound field using an open Kirchhoff surface. AIAA J. 34, 909–916.

Freund, J.B., Lele, S.K., Moin, P., 1998. Direct simulation of a Mach 1.92 jet and its sound field. AIAA Paper, AIAA-1998-2291.

Hussein, H.J., Capp, S.P., George, S.K., 1994. Velocity measurements in a high-Reynolds-number, momentum-conserving, axisymmetric turbulent jet. J. Fluid Mech. 258, 31–75.

Lighthill, M.J., 1952. On sound generated aerodynamically. I. General theory. Proc. Royal Soc. A 211, 564–587.

Lush, P.A., 1971. Measurements of subsonic jet noise and comparison with theory. J. Fluid Mech. 46, 477–500.

Oran, E.S., Boris, J.P., 2001. Numerical Simulation of Reactive Flow, second ed. Cambridge University Press, Cambridge, MA.

Panchapakesan, N.R., Lumley, J.L., 1993. Turbulence measurements in axisymmetric jets of air and helium. Part I. Air jet. J. Fluid Mech. 246, 197–223.

Roe, P.L., 1981. Approximate Rieman solvers, parameter vectors and difference schemes. J. Comput. Phys. 46, 357–378.

Shur, M., Spalart, P.R., Strelets, M., Travin, A., 1999. Detached-eddy simulation of an airfoil at high angle of attack. In: Rodi, W., Laurence, D. (Eds.), Fourth Int. Symp. Eng. Turb. Modelling and Measurements. Elsevier, Amsterdam, pp. 669–678.

Spalart, P.R., Jou, W.-H., Strelets, M., Allmaras, S.R., 1997. Comments on the feasibility of LES for wings, and on a hybrid RANS/LES approach. In: Liu, C., Liu, Z. (Eds.), Advances in DNS/LES. Greyden Press, Columbus, OH.

Strelets, M., 2001. Detached-eddy simulation of massively separated flows. AIAA Paper, AIAA-2001-0879.

Stromberg, J.L., McLaughlin, D.K., Troutt, T.R., 1980. Flow field and acoustic properties of a Mach number 0.9 jet at a low Reynolds number. J. Sound Vib. 72, 159–176.

Tanna, H.K., 1977. An experimental study of jet noise. Part I. Turbulent mixing noise. J. Sound Vib. 50, 405–428.

Zaman, K.B.M., 1998. Asymptotic spreading rate of initially compressible jets—experiment and analysis. Phys. Fluids 10, 2652–2660.

Zhao, W., Frankel, S.H., Mongeau, L., 2000. Effects of spatial filtering on sound radiation from a subsonic axisymmetric jet. AIAA J. 38, 2032–2039.

Zhao, W., Frankel, S.H., Mongeau, L., 2001. Large eddy simulations of sound radiation from a subsonic axisymmetric jet. AIAA J. 39, 1469–1477.